Supporting Information

Engineering Copper Plasmonic Chirality via Ligand Induced Dissolution for Enantioselective Recognition of Amino Acids

*Sonia Maniappan,[a] Camelia Dutta ,[a] Arunima Cheran,[a] Diego M. Solís,[b] and Jatish Kumar [a]**

[a]*Department of Chemistry, Indian Institute of Science Education and Research (IISER) Tirupati, Tirupati 517507, India*
[b]*Departamento de Tecnología de los Computadores y de las Comunicaciones, University of Extremadura 10003 Cáceres, Spain*

E-mail: jatish@iisertirupati.ac.in

Table of Contents

Experimental Section

Chemicals: Copper chloride dihydrate ($CuCl_2 \cdot 2H_2O$, 99.9%), L-cysteine hydrochloride monohydrate, and sodium hydroxide were purchased from Sigma-Aldrich, TCI chemicals and SRL, respectively. L- and D-histidine, D-cysteine hydrochloride monohydrate, tryptophan, tyrosine, methionine, serine and L-DOPA were purchased from TCI chemicals. All the chemicals were commercially obtained and used without further purification. All the glassware used in synthesis were washed thoroughly in aqua regia prior to use. Deionized water was used in the preparation of aqueous solution of the samples.

Synthesis of chiral Cu nanoparticles (CuNPs): Chiral CuNPs were synthesized using the following procedure: A 10 mL solution containing L-cysteine (10 mM) and NaOH (5 mM) was added to a 10 mL aqueous solution of $CuCl_2.2H_2O$ (10 mM). The resulting solution was vigorously stirred at 500 rpm for a duration of 10 min. To purify the CuNPs, centrifugation was performed at 6000 rpm for 10 min. The purification process involved three cycles of washing with water and ethanol, followed by centrifugation. The copper nanoparticles were then vacuum dried at 35°C for 12 h and stored at 4°C for future use.

Formation of Cu-histidine complex from CuNPs: In the experimental procedure, 100µL of CuNPs were initially placed in a cuvette. Subsequently, histidine was incrementally added, and the CD signals were monitored at each step. The addition process proceeded until the histidine concentration reached 3.7 mM, resulting in a complete inversion of the CD signals.

Crystallization of the formed Cu-histidine complex: The formation of Cu-histidine complex was accompanied by the appearance of deep blue coloured solution. The crystals for SCXRD analysis were obtained using vapour diffusion technique by dissolving the compound in 1:1 ratio of water-ethanol. The vapour diffusion was carried out in presence of acetone and blue crystals were obtained by leaving the sample undisturbed for one week.

Characterization: Size and morphology of the nanoparticles was analyzed using TEM imaging and were captured in FEI Tecnai G2 60-3000 microscope with an acceleration voltage of 300 kV. Powder X-ray diffraction pattern was recorded using PANalytical X-ray diffractometer with CuKa

radiation (1.5406 A) in the range of 10–80^0 (2θ) at a scanning rate of 0.1^0/ min. UV-vis absorption studies were carried out Agilent Cary 3500 UV-vis multicell Peltier and CD measurements were analyzed using JASCO J-1500 CD spectrophotometer. The FT-IR spectrum was collected on PerkinElmer Spectrum Two FT-IR spectrometer. SCXRD was recorded on Bruker D8 VENTURE Super DUO Diffractometer with PhotonIII Detector. XPS measurement was carried out using an ESCA Plus spectrometer (Omicron Nanotechnology Ltd, Germany using Mg-Kα source). Raman studies were performed on Horiba LabRam 800 spectrophotometer with a Peltier-cooled charge couple (CCD) detector. He-Ne laser with 488 nm laser was used as the excitation source.

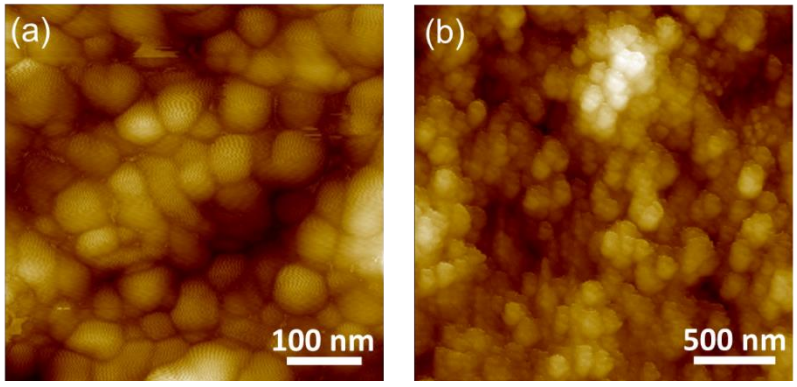

Fig. S1 Representative AFM images of CuNPs synthesized using (a) L-cysteine and (b) D-cysteine as the capping agent.

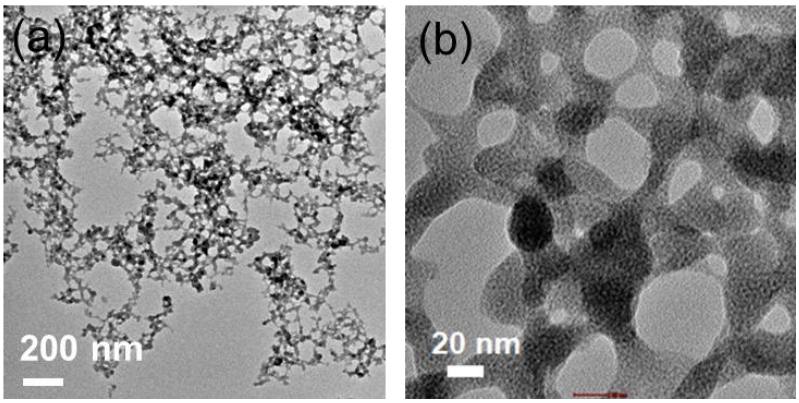

Fig. S2 TEM images of L-CuNPs at different magnifications.

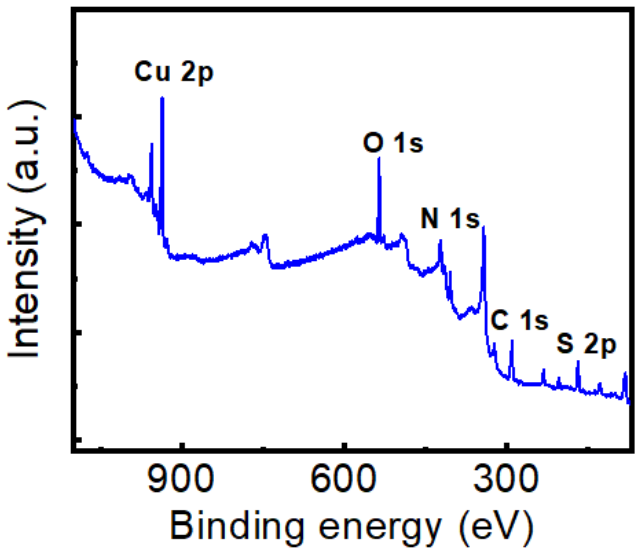

Fig. S3 XPS survey spectra of L-CuNPs.

Table S1. Composition of different elements present in L-CuNPs calculated from XPS.

Atom	Atomic percentage (%)
Cu	9.16
O	20.25
N	13.19
S	21.28
Cl	2.82
C	33.31

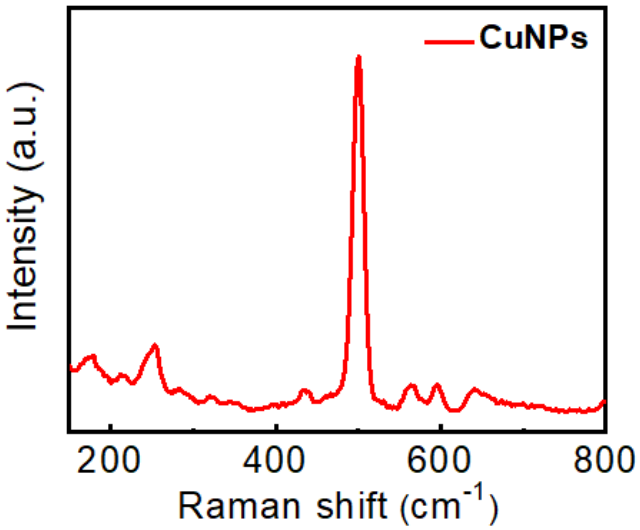

Fig. S4 Raman spectra of L-CuNPs.

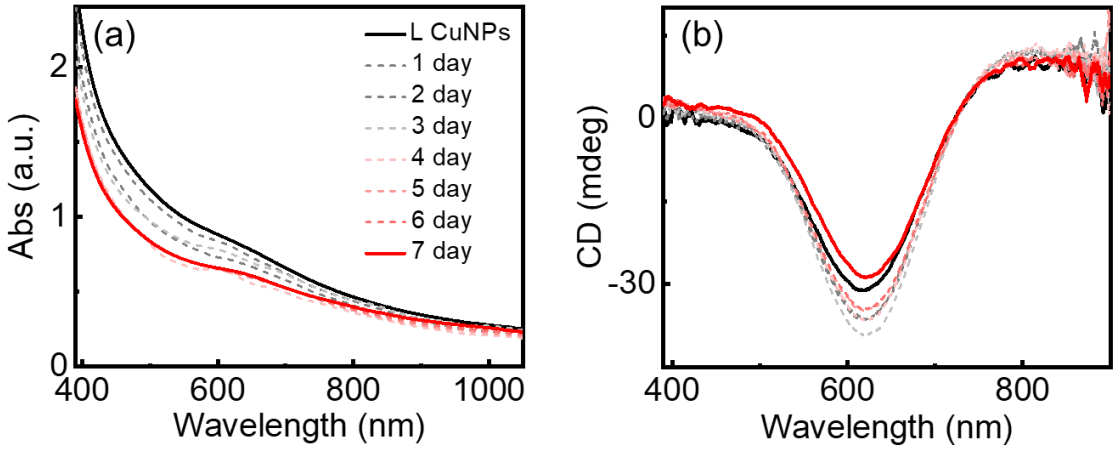

Fig. S5 Stability of L-CuNPs monitored through (a) UV-visible and (b) CD spectral changes for a period of 7 days.

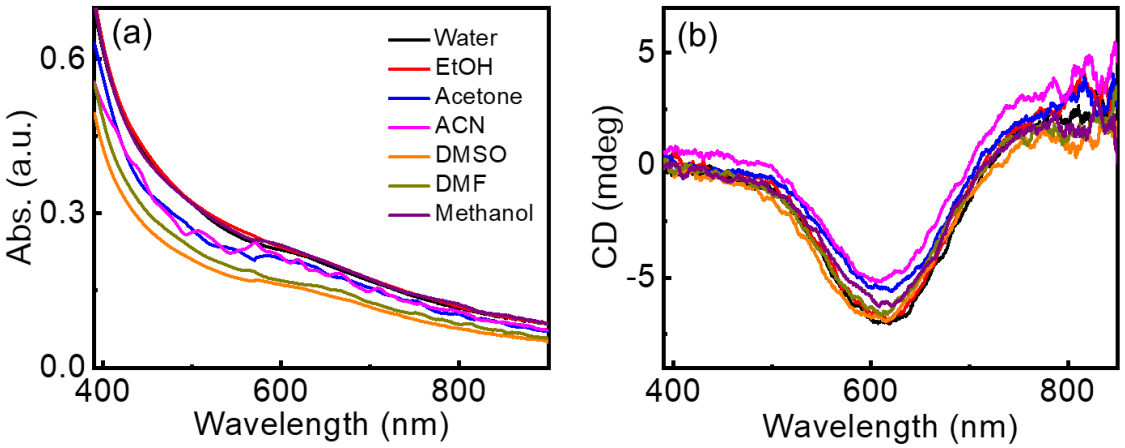

Fig. S6 (a) UV-visible and (b) CD spectra of L-CuNPs collected after dispersing in solvents of varying polarity.

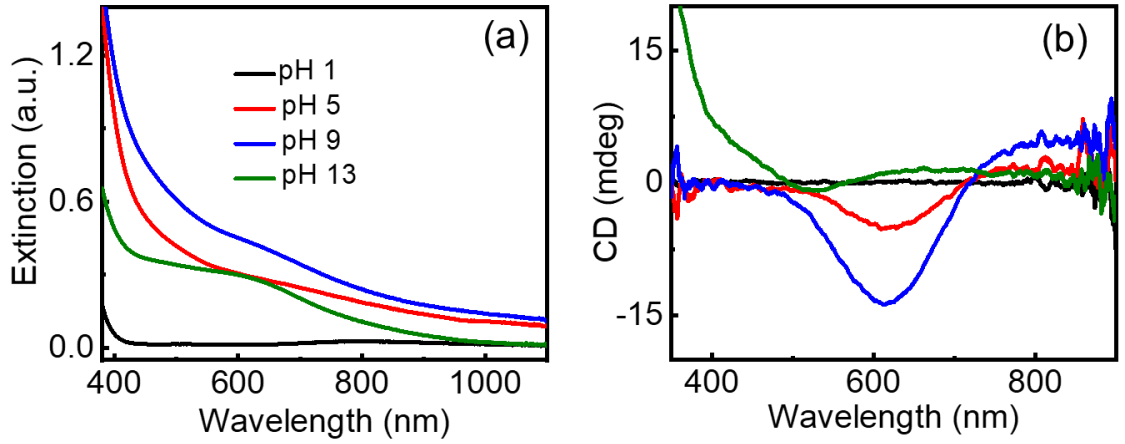

Fig. S7 (a) UV-visible and (b) CD spectra of L-CuNPs at varying pH.

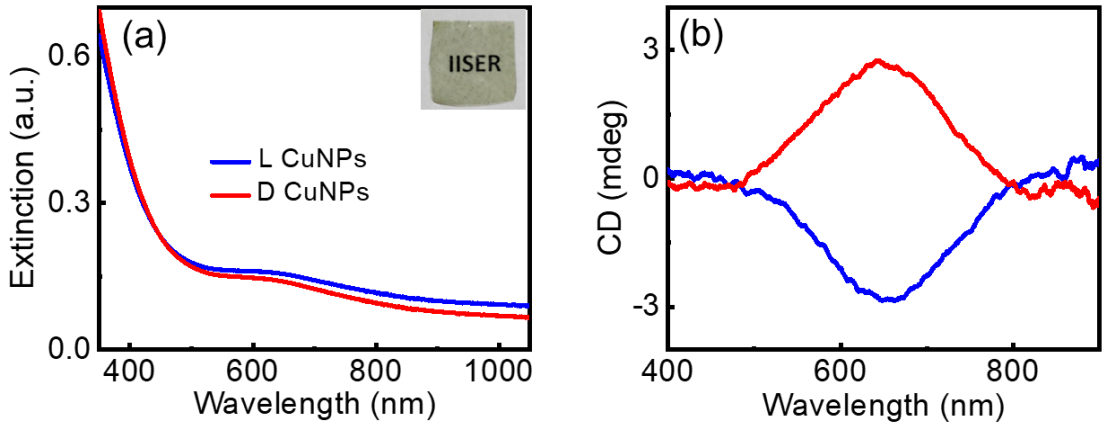

Fig. S8 Solid state CD spectra of L- (black trace) and D-CuNPs (red trace) incorporated in PVA film. Inset in (a) shows the photographic image of self-standing film.

Theoretical studies:

The Cu nanoparticles' approximately spherical shape justifies the assumption of Mie theory's perfectly spherical model.[1] In order to include the cysteine layer's isotropic chiroptical activity into such model, we extend the usual macroscopic constitutive relations of electric permittivity ϵ and magnetic permeability μ

$$\mathbf{D} = \epsilon\mathbf{E}, \qquad \mathbf{B} = \mu\mathbf{H},$$

by adopting the Drude-Born-Fedorov constitutive relations: [2]

$$\mathbf{D} = \epsilon(\mathbf{E} + \alpha\, \boldsymbol{\nabla} \times \mathbf{E}), \qquad \mathbf{B} = \mu(\mathbf{H} + \alpha\, \boldsymbol{\nabla} \times \mathbf{H}),$$

where the phenomenological scalar parameter α multiplying the curl operator $\boldsymbol{\nabla} \times$ quantifies the macroscopic strength of the chiral response and, implicitly, the underlying magnetoelectric coupling. Importantly, as in any other bi-isotropic medium, there are two uncoupled plane-wave eigenmodes that can propagate with unaltered state of polarization: right- and left-hand elliptical (here, circular) polarizations, which we denote with R/L subscripts. These two states experiment different propagation constants:[3]

$$k_{R/L} = k\,\frac{1 \mp \alpha\, k}{1-(\alpha\, k)^2},$$

$k = \omega\sqrt{\mu\epsilon}$ being the usual propagation constant when $\alpha = 0$, which we can heuristically relate to a pair of effective dielectric constants $\epsilon_{R/L}$ satisfying $k_{R/L} = \omega\sqrt{\mu\epsilon_{R/L}}$. Such effective values of the dielectric permittivity of cysteine have been parameterized in the literature with a single-resonance model[4] that allows us to derive:

$$\alpha = \frac{1}{2}\left(\frac{1}{k_R} - \frac{1}{k_L}\right), \qquad \sqrt{\epsilon} = 2\left(\frac{1}{\sqrt{\epsilon_R}} + \frac{1}{\sqrt{\epsilon_L}}\right)^{-1}.$$

In our case, $\epsilon_{R/L}$ is actually the result of applying Maxwell-Garnett effective medium theory[5] to the Cu/cysteine shell compound, with a Cu volume fraction in the range [0.15,0.35]. Cu is described by the complex permittivity obtained from optical measurements in ref. 6.

In order to quantify the chiral response of our ideal CuNP, we first define circular dichroism (CD) and optical rotation (OR) as the amount of change in ellipticity and azimuth, respectively, of a horizontally (linearly) polarized incident beam as it passes through the sample, assuming propagation along z.[1] The former is associated to the difference in the imaginary part of the refractive indices of L- and R- polarizations, whereas the latter relates to their real part, assuming homogeneous media. In our case, we have an aggregate of nanoparticles and, for the sake of simplicity, we will assume that their volume density within the solution is low enough to discard the electromagnetic coupling among them. We choose a 5% volume fraction of the particles diluted in water (the average distance between consecutive CuNPs is roughly more than twice their size along the three dimensions), which amounts to $N = 7.94 \times 10^{20}$ particles per cubic meter. Under such assumptions, we can write:[1,3]

$$CD \approx +\frac{\pi N h}{k_{water}^2} Re\{S_L - S_R\}, \qquad OR \approx -\frac{\pi N h}{k_{water}^2} Im\{S_L - S_R\},$$

where h is the sample thickness (we choose 1μm in our calculations), and S_L and S_R stand for the forward scattering matrix elements in the circular basis.[3]

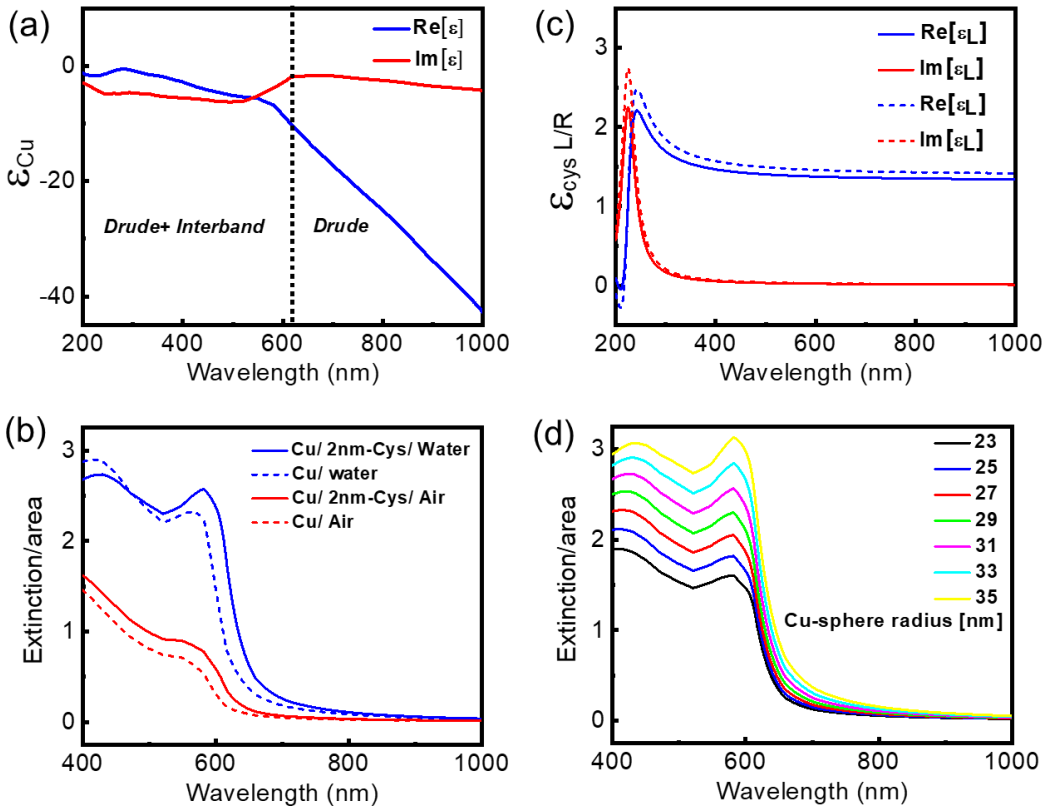

Fig. S9 (a,b) Relative permittivity vs. wavelength of Cu and cysteine, respectively. (c) Extinction efficiency vs. wavelength of the Cu nanosphere with and without the cysteine layer, immersed in water and air. (d) Extinction efficiency for different radii of the Cu core sphere, with fixed 2 nm thickness of the cysteine shell and $f_{Cu/Cys} = 0.25$.

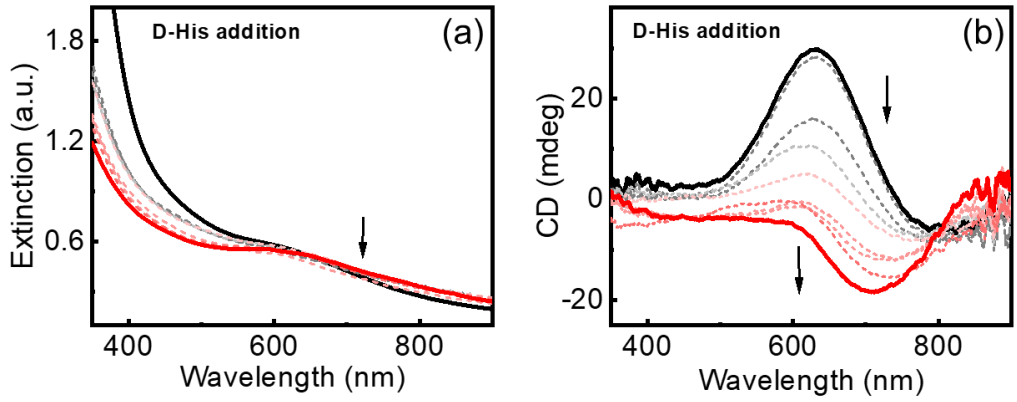

Fig. S10 (a) UV-visible and (b) CD spectral changes of D-CuNPs with the sequential addition of D-histidine.

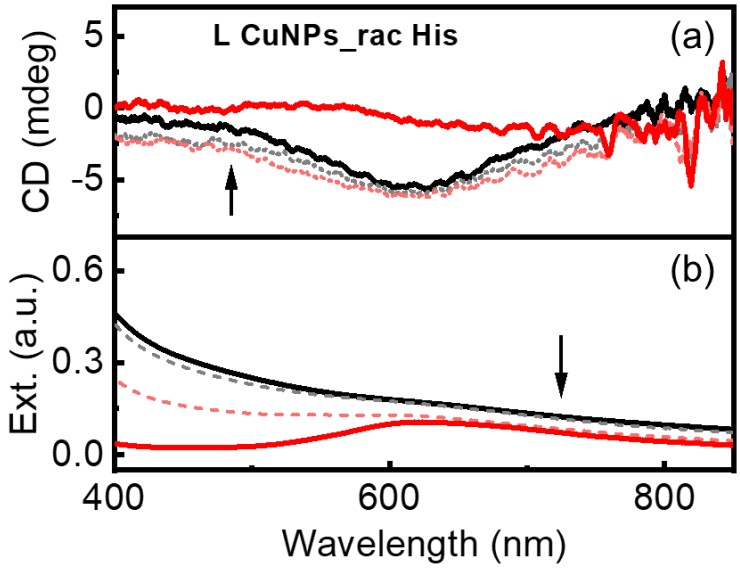

Fig. S11 (a) UV-visible and (b) CD spectral changes of L-CuNPs on the addition of racemic mixture of histidine.

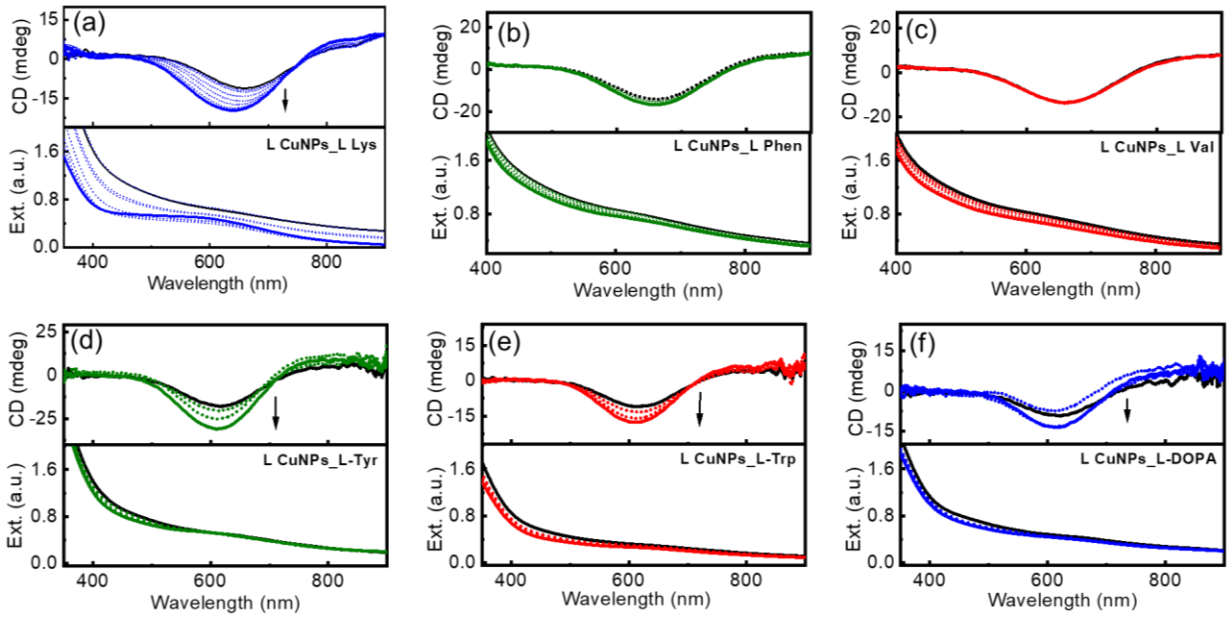

Fig. S12 UV-visible (top) and CD (bottom) spectral changes of L-CuNPs on interaction with different amino acids; (a) L-lysine, (b) L-phenylalanine, (c) L-valine, (d) L-tyrosine, (e) L-tryptophan and (f) L-DOPA.

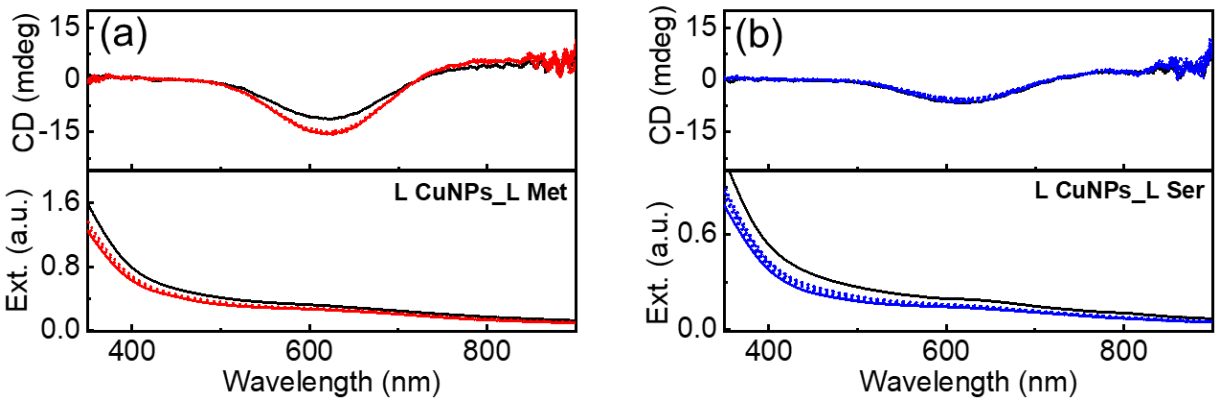

Fig. S13 UV-visible (top) and CD (bottom) spectral changes of L-CuNPs on interaction with (a) methionine and (b) serine.

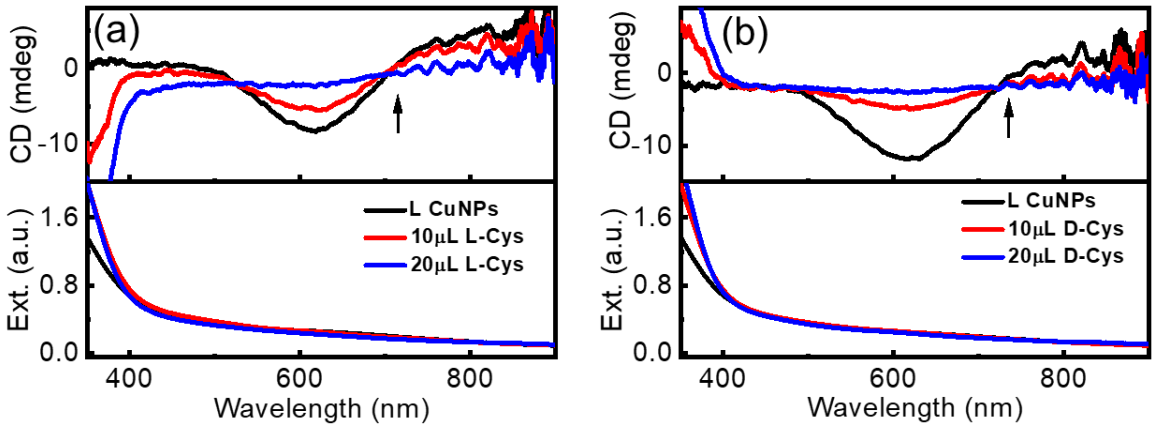

Fig. S14 Changes in the UV-visible (top) and CD (bottom) spectral profile of L-CuNPs on the addition of (a) L-cysteine and (b) D-cysteine.

Table S2. Table containing crystallographic parameters

	D-His_Cu complex	**L-His_Cu complex**
X-Ray source	Monochromatic Mo	Monochromatic Mo
Method	Intrinsic Phasing 1	Intrinsic Phasing 1
Space group	$P3_221$ (Monoclinic)	$P3_121$ (Monoclinic)
Cell length a	10.9067(8)	10.8811(12)
Cell length b	10.9067(8)	10.8811(12)
Cell length c	31.970(4)	31.653(5)
Cell angle alpha	90^0	90^0
Cell angle beta	90^0	90^0
Cell angle gamma	120^0	120^0
Cell volume	3293.5(6)	3245.5(9)
Cell measurement temperature	100K	100K
R_1	6.77 %	5.76 %
wR_2	16.31 %	14.47 %
Completeness	100%	99.9%
Shift	0.001	0.001
Crystal colour	Clear dark blue	Clear dark blue

Theoretical simulation of the complex:

Theoretically the structure of obtained histidine copper complex was optimized from the single crystal structure through density functional theory (DFT) calculations by adopting the basis set def2svp and functional pbe1pbe. Theoretically optimized lowest energy configuration of the complex (Figure S15) yielded similar excitation and CD profile when computed with time dependent density functional theory (TD-DFT) calculations (Figure S16). However, the minor deviation observed in the peak position may be due to the limited number of excited states used for the calculations. In addition to TD-DFT, natural bond orbital (NBO) calculations were carried

out in order to visualize the highest occupied molecular orbital (HOMO) and lowest unoccupied molecular orbital (LUMO). Def2svp and pbe1pbe was used as the basis set and functional, respectively, to carry out the NBO calculations. NBO calculation revealed the HOMO and LUMO both are centered on d orbitals leading to d-d transition responsible for the electronic absorption. The HOMO is observed to be stabilized by 0.1737 eV from the LUMO. Figure S17 represents the orbital diagram of LUMO+1, LUMO, HOMO, HOMO-1.

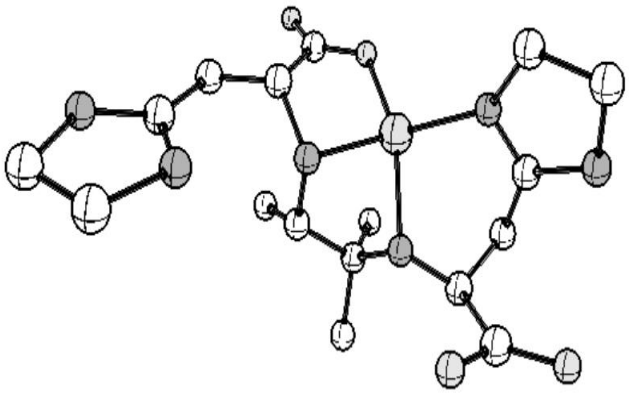

Fig. S15 Energy minimized structure of copper histidine complex.

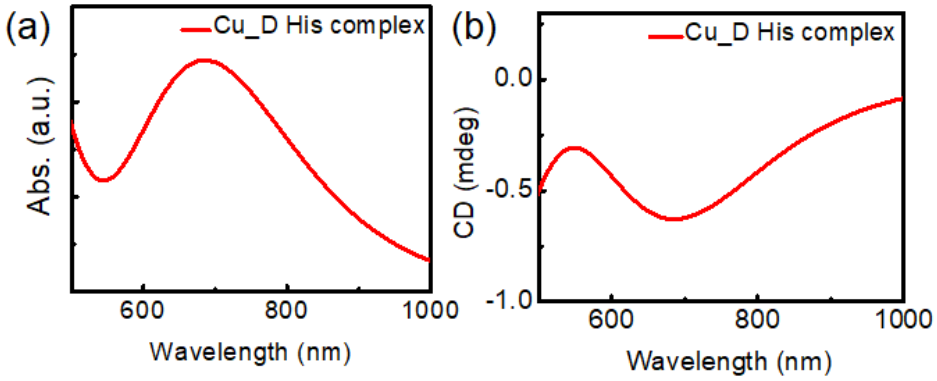

Fig. S16 Simulated (a) absorption and (b) ECD spectra of D-histidine coordinated copper complex

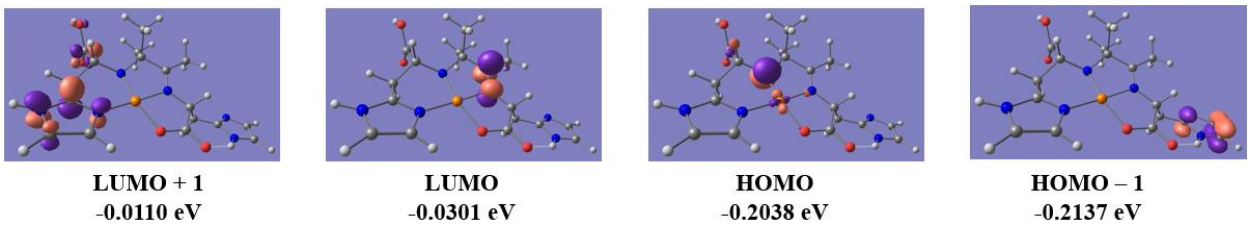

Fig. S17 Selected frontier molecular orbital diagram of copper histidine complex at its lowest energy optimized geometry.

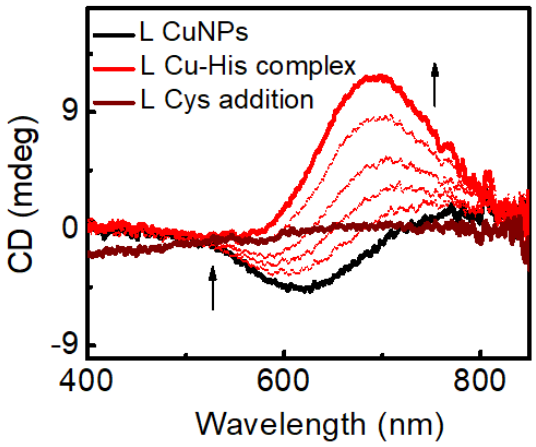

Fig. S18 CD spectral changes of L-CuNPs depicting the formation of complex on addition of L-histidine (red traces) and the subsequent spectral changes upon addition of L-cysteine to the formed complex (brown trace).

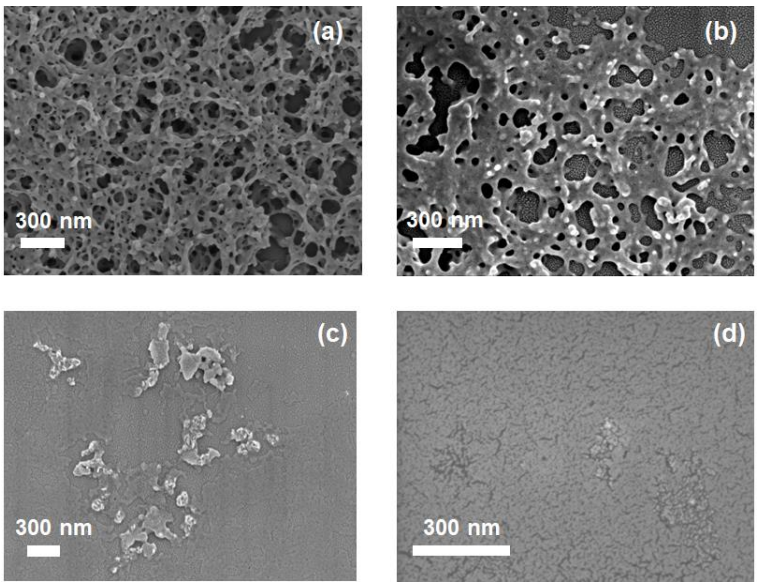

Fig. S19 SEM images of different stages of L-histidine addition to L-CuNPs; (a) 0 mM, (b) 1 mM, (c) 2.8 mM, and (d) 3.7 mM.

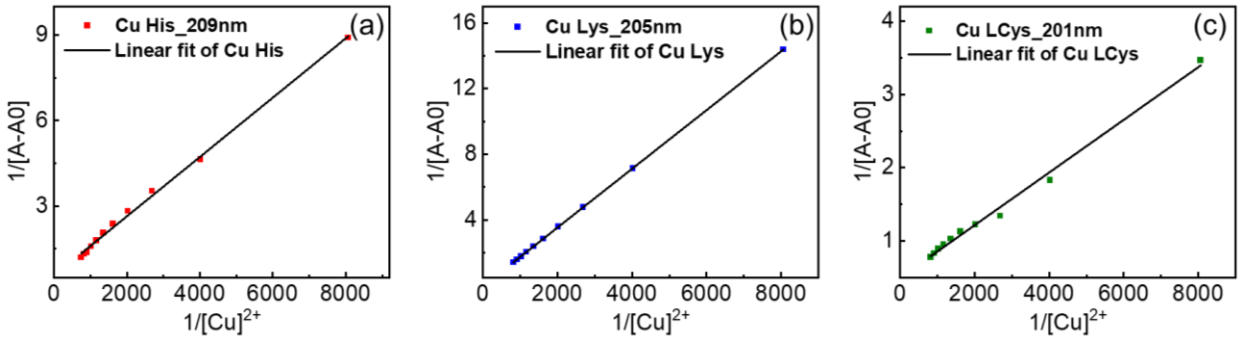

Fig. S20 Benesi-Hildebrand plots for determination of binding constant of copper complex with amino acids, (a) L- histidine, (b) L-lysine and (c) L-cysteine.

References

1. C. F. Bohren and D. R. Huffman, *Absorption and scattering of light by small particles*, John Wiley & Sons, 2008.

2. I. Lindell, A. Sihvola, S. Tretyakov and A. J. Viitanen, *Electromagnetic waves in chiral and bi-isotropic media*, Artech House 1994.

3. C. F. Bohren, Scattering of electromagnetic waves by an optically active spherical shell, *J. Chem. Phys.*, 1975, **62**, 1566-1571.

4. G. Zheng, Z. Bao, J. Pérez-Juste, R. Du, W. Liu, J. Dai, W. Zhang, L. Y. S. Lee and K. Y. Wong, Tuning the morphology and chiroptical properties of discrete gold nanorods with amino acids, *Angew. Chem. Int. Ed.*, 2018, **57**, 16452-16457.

5. G. A. Niklasson, C. G. Granqvist and O. Hunderi, Effective medium models for the optical properties of inhomogeneous materials, *Appl. Opt.*, 1981, **20**, 26-30.

6. P. B. Johnson and R. W. Christy, Optical constants of the noble metals, *Phys. Rev. B*, 1972, **6**, 4370.